International Journal of Fracture **86:** 221–245, 1997.

Computing edge singularities in elastic anisotropic three-dimensional domains

ZOHAR YOSIBASH
Pearlstone Center for Aeronautical Engineering Studies, Department of Mechanical Engineering, Ben-Gurion University of the Negev, Beer-Sheva 84105, Israel

Received 6 February 1997; accepted in revised form 30 July 1997

Abstract. Computation of eigen-pairs characterizing the linear elastostatic solution in three-dimensional anisotropic domains in the vicinity of edge singularities is addressed. The singularities may be caused by re-entrant corners, abrupt changes in boundary conditions or material properties. Edge singularities in three-dimensional domains are of great interest from the point of view of failure initiation: The eigen-pairs characterize the straining modes and their amplitudes quantify the amount of energy residing in particular straining modes. For this reason, failure theories directly or indirectly involve the eigen-pairs and their amplitudes.

Herein we address the problem of determining the edge eigen-pairs numerically on the basis of the modified Steklov formulation in conjunction with the p-version of the finite element method. The method is very accurate, efficient and robust, and provides complex eigen-pairs if they exist. Several practical problems are studied, and examples are presented for cases including multi-material inclusion problems, cracks in dissimilar materials, and multi-material interfaces at free and clamped edges.

Key words: Singularities, Finite Element Methods, Steklov method, multi-material interfaces, p-version, delamination, three-dimensional elasticity, fracture-mechanics.

1. Introduction

This paper addresses the mechanical response of linearly elastic three-dimensional domains, subject to small displacements, in the vicinity of edges. Edges are curves created by the intersection of surface boundaries of a three-dimensional domain, and in their neighborhood the stress tensor exhibits singular behavior, i.e. tends to infinity as the distance from the edge tends to zero.

Due to the complex treatment of three-dimensional edge singularities, most of the research on singular stress fields has focused on two-dimensional domains under the assumption of plane-stress or plane-strain. The reader is referred to the list of publications (Barsoum, 1988 to Costabel and Dauge, 1995; Dempsey and Sinclair, 1979; Gu and Belytschko, 1994 to Papadakis and Babuška, 1995; Ting, 1986; Williams, 1952; Ying, 1986 and Yosibash and Szabó, 1995) (not exhaustive by any means), and the references therein which address the analytical as well as numerical computation of eigen-pairs in two-dimensions.

Renewed interest in the solution of the three-dimensional linear elastic problems at edges occurred due to increasing interest in anisotropic laminated composites and electronic devices. The displacement solution (associated with the singular stress tensor) is uniquely characterized by a sequence of discrete eigen-pairs and their coefficients (in the neighborhood of edges). These are of great interest in structural mechanics because they provide a basis for predicting failure events in the vicinity of edges.

It is assumed that the edge of interest lays along a straight edge coinciding with the z Cartesian axis, with the geometry and material properties independent of it. Let us denote the

three displacement fields $\boldsymbol{u} \stackrel{\text{def}}{=} (u_x, u_y, u_z)^T$. In some cases, for instance isotropic domains as well as some special orthotropic domains (if in each sub-domain the orthotropy axis coincides with the z-axis), the problem for u_z is uncoupled with the problem for u_x, u_y. The two displacements u_x, u_y satisfy the genuine two dimensional elasticity problem, and u_z is a solution of an elliptic equation. However, for anisotropic domains, the problem of computing the edge eigen-pairs is fully coupled.

Three-dimensional edge singularities have been less investigated, especially when associated with anisotropic materials and multi-material interfaces. Analytical methods as in (Ting and Chou, 1981; Wang and Choi, 1982) provide the means for computing the eigen-pairs for a two-material interface however requires extensive mathematics. Several numerical methods, mainly based on the h-version of the finite element method have been suggested lately. Among them (Leguillon and Sanchez-Palencia, 1987), where a determinant method is developed for the computation of the eigen-pairs, (Gu and Belytschko, 1994) in which an excellent reference list to the subject is provided, and (Pageau and Biggers, 1996). These methods provide good results, and the eigen-pairs are obtained by solving a quadratic eigen-problem. An inherent difficulty associated with h- version FE methods is the fact that an adaptive scheme for assuring the convergence of the computed values is not always available. The applicability of the above methods is not demonstrated for displacements homogeneous boundary conditions, and it is felt that they fail to indicate these cases which give rise to power-logarithmic stress singularities.

Herein, a short description of new procedures for computing the edge eigen-pairs, limited to the most essential features are briefly outline in Section 2, whereas the full details are provided in (Yosibash, 1997b). In Section 3 numerical examples are provided.

New results on the performance of the numerical algorithms applied to problems at multi-material internal interfaces, and fixed-free edges are reported herein for the first time. These include edge crack singularities at a bi-material anisotropic interface, free edge effects in a two cross-ply anisotropic laminate, a multi-material internal interface, and composite patches bonded to a metallic structure. The obtained eigen-pairs are compared to the exact values when available, demonstrating the efficiency, accuracy and robustness of the method. We conclude with conclusions in Section 4.

2. Formulating the eigen-problem

The elastostatic displacements field in three-dimensions, in the vicinity of an edge (which is sufficiently away from a vertex) can be decomposed in terms of edge eigen-pairs and edge stress intensity functions (ESIFs). Mathematical details on the decomposition can be found e.g. in (Dauge, 1988; Andersson et al., 1995; Grisvard, 1992) and the references therein. A representative three-dimensional domain denoted by Ω, which contains typical 3-D singularities is shown in Figure 1. Edge singularities arise in the neighborhood of the edges Λ_{ij} and these will be addressed in the following. It shall be assumed that curved edges which intersect at vertices do not exist, and that the crack faces, if any, lay in a flat plane.

In the neighborhood of an edge, we create a cylindrical domain of radius $r = R$ having the edge Λ_{ij} as its axis, see Figure 2. The displacements in the edge neighborhood can be decomposed as follows

$$\boldsymbol{u}(r,\theta,z) = \sum_{k=1}^{K} \sum_{s=0}^{S} a_{ks}(z) r^{\alpha_k} (\ln r)^s \boldsymbol{f}_{ks}(\theta) + \boldsymbol{w}(r,\theta,z), \tag{1}$$

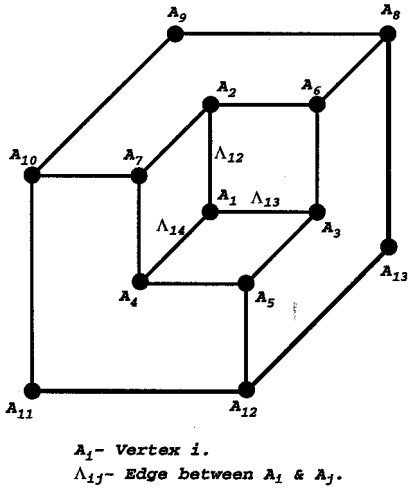

Figure 1. Typical 3-D singularities.

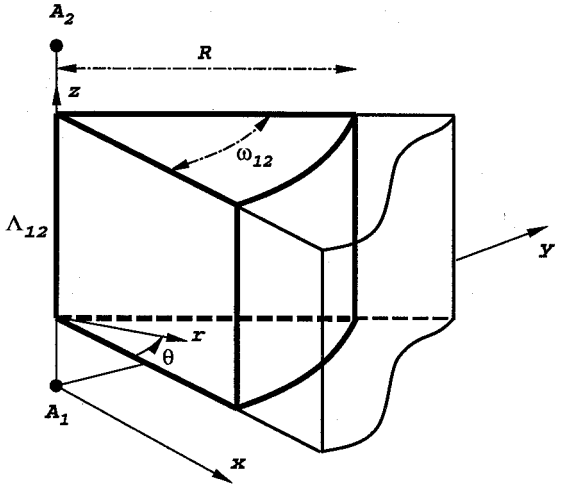

Figure 2. The edge neighborhood.

where $S \geqslant 0$ is an integer which is zero for most practical problems, except for special cases, $\alpha_{k+1} \geqslant \alpha_k$ are called edge eigen-values, $a_{ks}(z)$ are analytic in z called edge stress intensity functions (ESIFs), and can become very large as they approach one of the vertices, and $\boldsymbol{f}_{ks}(\theta)$ are analytic in θ, called edge eigen-functions. The vector function $\boldsymbol{w}(r, \theta, z)$ belongs to $[H^2]^3$ (H denotes the usual Sobolev space in one-dimension). We shall address herein only these cases where $S = 0$, therefore, (1) becomes

$$\boldsymbol{u}(r, \theta, z) = \sum_{k=1}^{K} a_k(z) r^{\alpha_k} \boldsymbol{f}_k(\theta) + \boldsymbol{w}(r, \theta, z). \tag{2}$$

$\boldsymbol{u} = (u_x\, u_y\, u_z)^T$ is the displacements vector, with $u_x(r, \theta, z)$, $u_y(r, \theta, z)$ and $u_z(r, \theta, z)$ being its components in the x, y and z directions respectively. We denote the tractions on the boundaries by $\boldsymbol{T} = (T_x\, T_y\, T_z)^T$. In the vicinity of the edge we assume that no body forces are present.

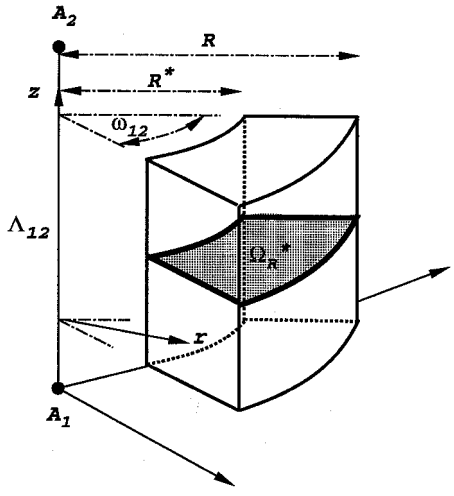

Figure 3. The modified Steklov domain Ω_R^*.

A *two-dimensional* sub-domain is constructed which is in a plane perpendicular to the edge (z-axis) and bounded by the radii $r = R^*$ and $r = R$. This domain, denoted by Ω_R^*, is shown in Figure 3.

On the boundaries $\theta = 0$ and $\theta = \omega_{ij}$ of the sub-domain Ω_R^* either homogeneous traction boundary conditions ($\boldsymbol{T} = \boldsymbol{0}$), or homogeneous displacements boundary conditions, or a combination of these are prescribed.

In view of (2), $\boldsymbol{u}$ in Ω_{R^*} (respectively $\boldsymbol{v}$) has the functional representation

$$\boldsymbol{u} \stackrel{\text{def}}{=} A(z)r^{\alpha} \left\{ \begin{array}{c} f_x(\theta) \\ f_y(\theta) \\ f_z(\theta) \end{array} \right\} = A(z)r^{\alpha}\boldsymbol{f}(\theta), \quad \boldsymbol{v} \stackrel{\text{def}}{=} B(z)r^{\alpha}\boldsymbol{f}(\theta). \tag{3}$$

We also denote the *in-plane* variation of the displacements as follows

$$\tilde{\boldsymbol{u}}(r,\theta) \stackrel{\text{def}}{=} \boldsymbol{u}/A(z) \quad \tilde{\boldsymbol{v}}(r,\theta) \stackrel{\text{def}}{=} \boldsymbol{v}/B(z). \tag{4}$$

Following the steps presented in detail in (Yosibash, 1997), an eigen-problem is cast in a weak form which is an integral equation over a two dimensional domain involving the three displacement fields. This weak formulation is called the weak *Modified Steklov* form

$$\begin{aligned} &\textbf{Seek } \alpha \in \mathcal{C}, \boldsymbol{0} \neq \tilde{\boldsymbol{u}} \in [H^1(\Omega_R^*)]^3, \quad \text{such that,} \quad \forall \tilde{\boldsymbol{v}} \in [H^1(\Omega_R^*)]^3 \\ &\quad \mathcal{B}(\tilde{\boldsymbol{u}},\tilde{\boldsymbol{v}}) - [\mathcal{N}_R(\tilde{\boldsymbol{u}},\tilde{\boldsymbol{v}}) - \mathcal{N}_{R^*}(\tilde{\boldsymbol{u}},\tilde{\boldsymbol{v}})] = \alpha[\mathcal{M}_R(\tilde{\boldsymbol{u}},\tilde{\boldsymbol{v}}) - \mathcal{M}_{R^*}(\tilde{\boldsymbol{u}},\tilde{\boldsymbol{v}})] \end{aligned} \tag{5}$$

Ω_R^* is the two dimensional domain which is the flat surface bounded by $0 \leqslant \theta \leqslant \omega_{12}$ and $R^* \leqslant r \leqslant R$ as shown in Figure 3, and

$$\mathcal{B}(\tilde{\boldsymbol{u}},\tilde{\boldsymbol{v}}) \stackrel{\text{def}}{=} \int_{R^*}^{R}\int_0^{\omega_{12}} \left\{ \left([A_r]\partial_r + [A_\theta]\frac{\partial_\theta}{r} \right) \tilde{\boldsymbol{v}} \right\}^T [E] \left\{ \left([A_r]\partial_r + [A_\theta]\frac{\partial_\theta}{r} \right) \tilde{\boldsymbol{u}} \right\} r \, \mathrm{d}\theta \, \mathrm{d}r \tag{6}$$

$$\mathcal{N}_R(\tilde{\boldsymbol{u}},\tilde{\boldsymbol{v}}) \stackrel{\text{def}}{=} \int_0^{\omega_{12}} \tilde{\boldsymbol{v}}^T [A_r]^T [E][A_\theta]\partial_\theta \tilde{\boldsymbol{u}} \Big|_{r=R} \mathrm{d}\theta \tag{7}$$

$$\mathcal{M}_R(\tilde{\boldsymbol{u}},\tilde{\boldsymbol{v}}) \stackrel{\text{def}}{=} \int_0^{\omega_{12}} \tilde{\boldsymbol{v}}^T [A_r]^T [E][A_r]\tilde{\boldsymbol{u}}\Big|_{r=R} \mathrm{d}\theta. \tag{8}$$

where,

$$[A_r] \stackrel{\text{def}}{=} \begin{bmatrix} \cos\theta & 0 & 0 \\ 0 & \sin\theta & 0 \\ 0 & 0 & 0 \\ \sin\theta & \cos\theta & 0 \\ 0 & 0 & \sin\theta \\ 0 & 0 & \cos\theta \end{bmatrix} \quad [A_\theta] \stackrel{\text{def}}{=} \begin{bmatrix} -\sin\theta & 0 & 0 \\ 0 & \cos\theta & 0 \\ 0 & 0 & 0 \\ \cos\theta & -\sin\theta & 0 \\ 0 & 0 & \cos\theta \\ 0 & 0 & -\sin\theta \end{bmatrix} \tag{9}$$

and $[E]$ is the 6×6 symmetric material matrix connection the strain vector $\varepsilon = (\varepsilon_x\, \varepsilon_y\, \varepsilon_z\, \gamma_{xy}\, \gamma_{yz}\, \gamma_{xz})^T$ to the stress vector $\boldsymbol{\sigma} = (\sigma_x\, \sigma_y\, \sigma_z\, \tau_{xy}\, \tau_{yz}\, \tau_{xz})^T$.

REMARK 1. *Although the test and trial functions have three components, the domain over which the weak eigen-formulation is defined is two-dimensional, and excludes any singular points. Therefore the application of the p-version of the FEM for solving* (5) *is expected to be very efficient.*

REMARK 2. *The bilinear forms $\mathcal{N}_R$ and $\mathcal{N}_{R^*}$ are* non-symmetric *with respect to $\tilde{\boldsymbol{u}}$ and $\tilde{\boldsymbol{v}}$, thus is not self-adjoint. As a consequence, the 'minimax principle' does not hold, and any approximation of the eigenvalues (obtained using a finite dimension supspace of $[H^1(\Omega_R^*)]^3$) cannot be considered as an upper bound of the exact ones and the monotonic behavior of the error is lost as well. Never-the-less, convergence is assured (with a very high rate as will be shown by the numerical examples) under a general proof provided in* (Babuška and Aziz, 1972).

REMARK 3. *Note that in* (5) *we do not limit the domain Ω_R^* to be isotropic, and in fact* (5) *can be applied to multi-material anisotropic interface, as will be demonstrated by numerical examples.*

REMARK 4. *When homogeneous displacement boundary conditions are applied, one has to restrict the spaces to $[H_0^1(\Omega_R^*)]^3$, or a variation of it, so as to apply the essential boundary condition restrictions on the spaces in which $\tilde{\boldsymbol{u}}$ and $\tilde{\boldsymbol{v}}$ lay.*

2.1. NUMERICAL TREATMENT BY THE FINITE ELEMENT METHOD

In the following, the weak eigen-formulation (5) is discretised by considering a finite dimensional sub-space of $[H^1(\Omega_R^*)]^3$, employing the p-version of the finite element method.

Assume that the domain Ω_R^* consists of three different materials as shown in Figure 4. We divided Ω_R^* into, let's say 3 finite elements, through a meshing process. Let us consider a typical element, element number 1, shown in Figure 4, bounded by $\theta_1 \leqslant \theta \leqslant \theta_2$. A standard element in the ξ, η plane such that $-1 < \xi < 1, -1 < \eta < 1$ is considered, over which the polynomial basis and trial functions are defined. These standard elements are then mapped by

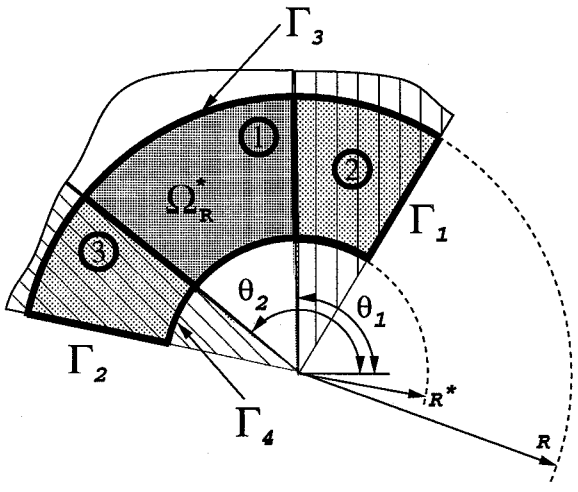

Figure 4. A typical finite element in the domain Ω_R^*.

appropriate mapping functions onto the 'real' elements (for details see (Szabó and Babuška, 1991), Chapter 5–6). The functions $\tilde{u}_x, \tilde{u}_y, \tilde{u}_z$ are expressed in terms of the basis functions $\Phi_i(\xi,\eta)$ in the standard plane

$$\left.\begin{aligned} \tilde{u}_x(\xi,\eta) &= \textstyle\sum_{i=1}^{N} a_i \Phi_i(\xi,\eta) \\ \tilde{u}_y(\xi,\eta) &= \textstyle\sum_{i=1}^{N} a_{N+i} \Phi_i(\xi,\eta) \\ \tilde{u}_x(\xi,\eta) &= \textstyle\sum_{i=1}^{N} a_{2N+i} \Phi_i(\xi,\eta) \end{aligned}\right\}, \tag{10}$$

or

$$\tilde{\boldsymbol{u}} = \begin{bmatrix} \Phi_1 \ \dots \ \Phi_N & 0 \ \dots \ 0 & 0 \ \dots \ 0 \\ 0 \ \dots \ 0 & \Phi_1 \ \dots \ \Phi_N & 0 \ \dots \ 0 \\ 0 \ \dots \ 0 & 0 \ \dots \ 0 & \Phi_1 \ \dots \ \Phi_N \end{bmatrix} \begin{Bmatrix} a_1 \\ \vdots \\ a_{3N} \end{Bmatrix} \stackrel{\text{def}}{=} [\Phi]\boldsymbol{a}, \tag{11}$$

where a_i are the amplitudes of the basis functions (sometimes called the 'nodal values'), and Φ_i are products of integrals of Legendre polynomials in ξ and η. $\tilde{\boldsymbol{u}}$ and $\tilde{\boldsymbol{v}}$ lay in the same space therefore, we define similarly $\tilde{\boldsymbol{v}} \stackrel{\text{def}}{=} [\Phi]\boldsymbol{b}$.

The unconstrained stiffness matrix corresponding to $\mathcal{B}(\tilde{\boldsymbol{u}}, \tilde{\boldsymbol{v}})$ on the typical element is given by

$$[K] \stackrel{\text{def}}{=} \int_{R^*}^{R} \int_{\theta_1}^{\theta_2} \left\{ \left([A_r]\partial_r + [A_\theta]\frac{\partial_\theta}{r} \right) [\Phi] \right\}^T [E] \left\{ \left([A_r]\partial_r + [A_\theta]\frac{\partial_\theta}{r} \right) [\Phi] \right\} r \, \mathrm{d}\theta \, \mathrm{d}r. \tag{12}$$

By defining the following matrices

$$[\partial P] \stackrel{\text{def}}{=} \begin{bmatrix} -P_1' \sin\theta & \dots & -P_N' \sin\theta & 0 & \dots & 0 & 0 & \dots & 0 \\ 0 & \dots & 0 & P_1' \cos\theta & \dots & P_N' \cos\theta & 0 & \dots & 0 \\ 0 & \dots & 0 & 0 & \dots & 0 & 0 & \dots & 0 \\ P_1' \cos\theta & \dots & P_N' \cos\theta & -P_1' \sin\theta & \dots & -P_N' \sin\theta & 0 & \dots & 0 \\ 0 & \dots & 0 & 0 & \dots & 0 & P_1' \cos\theta & \dots & P_N' \cos\theta \\ 0 & \dots & 0 & 0 & \dots & 0 & -P_1' \sin\theta & \dots & -P_N' \sin\theta \end{bmatrix}$$

$$[\tilde{P}] \stackrel{\text{def}}{=} \begin{bmatrix} P_1 \cos\theta & \dots & P_N \cos\theta & 0 & \dots & 0 & 0 & \dots & 0 \\ 0 & \dots & 0 & P_1 \sin\theta & \dots & P_N \sin\theta & 0 & \dots & 0 \\ 0 & \dots & 0 & 0 & \dots & 0 & 0 & \dots & 0 \\ P_1 \sin\theta & \dots & P_N \sin\theta & P_1 \cos\theta & \dots & P_N \cos\theta & 0 & \dots & 0 \\ 0 & \dots & 0 & 0 & \dots & 0 & P_1 \sin\theta & \dots & P_N \sin\theta \\ 0 & \dots & 0 & 0 & \dots & 0 & P_1 \cos\theta & \dots & P_N \cos\theta \end{bmatrix},$$

where $P_i(\xi)$ for $i > 3$ are integrals of Legendre polynomials, and $P_1(\xi) = (1-\xi)/2$, $P_2(\xi) = (1+\xi)/2$ (see for details (Szabó and Babuška, 1991), Chapter 3–6), we obtain the expression for $\mathcal{N}_R(\tilde{\boldsymbol{u}}, \tilde{\boldsymbol{v}})$

$$\mathcal{N}_R(\tilde{\boldsymbol{u}}, \tilde{\boldsymbol{v}}) = \boldsymbol{b}^T \left(\int_{-1}^{1} [\tilde{P}]^T [E] [\partial P] \Big|_{\eta=-1} \mathrm{d}\xi \right) \boldsymbol{a} \stackrel{\text{def}}{=} \boldsymbol{b}^T [N_R] \boldsymbol{a}. \tag{13}$$

The entries of $[N_R]$ are computed using Gauss quadrature.

Similarly, the expression $\mathcal{M}_R(\tilde{\boldsymbol{u}}, \tilde{\boldsymbol{v}})$ is evaluated by

$$\mathcal{M}_R(\tilde{\boldsymbol{u}}, \tilde{\boldsymbol{v}}) = \boldsymbol{b}^T \left(\frac{\theta_2 - \theta_1}{2} \int_{-1}^{1} [\tilde{P}]^T [E] [\tilde{P}] \Big|_{\eta=-1} \mathrm{d}\xi \right) \boldsymbol{a} \stackrel{\text{def}}{=} \boldsymbol{b}^T [M_R] \boldsymbol{a}. \tag{14}$$

The matrices $[N_{R^*}]$ and $[M_{R^*}]$ have same values as those of $[N_R]$ and $[M_R]$, but of opposite sign. This is because the shape functions on the artificial boundaries Γ_3 and Γ_4 are the same (except for some sign changes), and so is the mapping to the standard plane. Denoting the set of amplitudes of the basis functions associated with the artificial boundary Γ_3 by $\boldsymbol{a}_R$, and those associated with the artificial boundary Γ_4 by $\boldsymbol{a}_{R^*}$, the eigen-pairs can be obtained by solving the generalized matrix eigen-problem

$$[K]\boldsymbol{a} - ([N_R]\boldsymbol{a}_R - [N_{R^*}]\boldsymbol{a}_{R^*}) = \alpha([M_R]\boldsymbol{a}_R - [M_{R^*}]\boldsymbol{a}_{R^*}). \tag{15}$$

Augmenting the coefficients of the basis functions associated with Γ_3 with those associated with Γ_4, and denoting them by the vector $\boldsymbol{a}_{RR^*}$, (15) becomes

$$[K]\boldsymbol{a} - [N_{RR^*}]\boldsymbol{a}_{RR^*} = \alpha[M_{RR^*}]\boldsymbol{a}_{RR^*}. \tag{16}$$

We assemble the left hand part of (16). The vector which represents the total number of nodal values in Ω_R^* may be divided into two vectors such that one contains the coefficients

$\boldsymbol{a}_{RR^*}$, and the other contains the remaining coefficients: $\boldsymbol{a}^T = \{\boldsymbol{a}_{RR^*}^T,\ \boldsymbol{a}_{in}^T\}$. By partitioning $[K]$, we can write the eigen-problem (16) in the form

$$\begin{bmatrix} [K] - [N_{RR^*}] & [K_{RR^*-in}] \\ [K_{in-RR^*}] & [K_{in}] \end{bmatrix} \begin{Bmatrix} \boldsymbol{a}_{RR^*} \\ \boldsymbol{a}_{in} \end{Bmatrix} = \alpha \begin{bmatrix} [M_{RR^*}] & [0] \\ [0] & [0] \end{bmatrix} \begin{Bmatrix} \boldsymbol{a}_{RR^*} \\ \boldsymbol{a}_{in} \end{Bmatrix}. \tag{17}$$

The relation in (17) can be used to eliminate $\boldsymbol{a}_{in}$ by static condensation, thus obtaining the reduced eigen-problem

$$[K_S]\boldsymbol{a}_{RR^*} = \alpha[M_{RR^*}]\boldsymbol{a}_{RR^*}, \tag{18}$$

where

$$[K_S] = ([K] - [N_{RR^*}]) - [K_{RR^*-in}][K_{in}]^{-1}[K_{in-RR^*}].$$

It is possible to eliminate the unknowns $\boldsymbol{a}_{in}$ from the matrix $[K]$, because the relevant equations do not involve the as yet unknown eigenvalues α.

For the solution of the eigen-problem (18), it is important to note that $[K_S]$ is, in general, a full matrix. However, since the order of the matrices is relatively small, the solution (using Cholesky factorization to compute $[K_{in}]^{-1}$) is not expensive. The implementation issues for solving the generalized eigenvalue problem can be found in the LAPACK documentation (Anderson et al., 1994).

REMARK 5. *There is the possibility that m multiple eigenvalues exist with less than m corresponding eigenvectors (the algebraic multiplicity is higher than the geometric multiplicity). This is associated with the special cases when the asymptotic expansion contains power-logarithmic terms, and this behavior triggers the existence of* $\ln(r)$ *terms.*

REMARK 6. *Although we derived our matrices as if only one finite element exists along the boundary Γ_3 and Γ_4, the formulation for multiple finite elements is identical, and the matrices $[K], [N_R]$ and $[M_R]$ are obtained by an assembly procedure.*

REMARK 7. *In case of periodic boundary conditions, i.e. multi-material internal interfaces, the matrices $[K], [N_{RR^*}]$ and $[M_{RR^*}]$ are constrained according to* ((Leguillon and Sanchez-Palencia, 1987), p. 73).

Homogeneous displacements boundary conditions are applied by modifying the generated matrices. This is done by setting to zero only those rows and columns which correspond to the 'nodal variables' of the boundary conditions and then assigning the value of -1 to the relevant diagonal elements. This generates artificial eigen-values -1 with a multiplicity equal to the number of modified rows, however, negative integer eigen-values are not of interest in any case. As a result of the treatment, the order of the eigen-value problem to be solved is not reduced.

3. Numerical investigation

The modified Steklov weak-formulation is used in the following subsections for the investigation of the eigen-pairs occurring in several practical problems. Five different test cases are addressed:

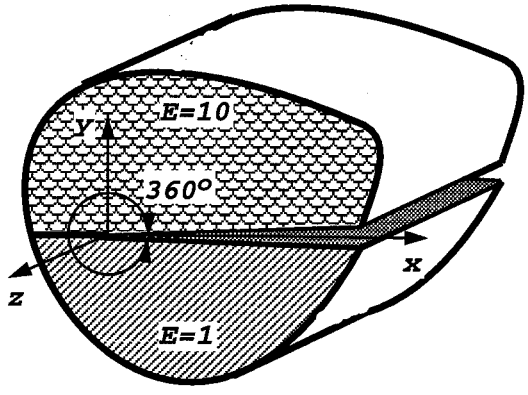

Figure 5. Plane crack at a bi-material interface.

(a) First, we consider a plane crack at the interface of a bi-material interface, for which analytical eigen-values exist, thus we may demonstrate the accuracy and efficiency of the method.

(b) Free edge effects in a two cross-ply anisotropic laminate are addressed, for which analytical eigen-values exist.

(c) An anisotropic multi-material internal interface.

(d) A composite patch terminating at different angles attached to a metallic structure.

(e) A composite patch attached to a metallic structure constrained against movement in the vertical direction.

In all example problems we use $R = 1$ and $R^* = 0.99$ (R^* has virtually no influence on the accuracy of the obtained eigen-pairs, and as $R^* \to 1$ the accuracy of the results slightly improves, see (Yosibash, 1997b)). Over each element in the used meshes the polynomial degree of the shape functions has been increased from 1 to 8.

3.1. PLANE CRACK AT A BI-MATERIAL INTERFACE

Consider a bi-material interface which is composed of two homogeneous materials, with continuity of tractions and displacements across interface maintained. The two materials are isotropic, both having Poisson ratio 0.3, the upper material having $E = 10$ and the lower $E = 1$ (E represents the Young modulus). We are interested in plane cracks at the interface of the two materials as shown in Figure 5. This example problem has been chosen to demonstrate the method's performance for cases where complex eigen-pairs arise. The exact first three eigen-pairs for this example problem are $\alpha_{1,2} = 0.5 \pm i0.07581177769$ and $\alpha_3 = 0.5$. In linear elastic fracture mechanics terminology α_1 and α_2 are associated with deformation in the $x - y$ plane (where mode I and mode II are coupled in this case), and α_3 is the out-of-plane mode.

The four-element mesh shown in Figure 6 has been used for the computations. The relative error (%) in the first two eigen-values is split in two: one defining the relative error in the real

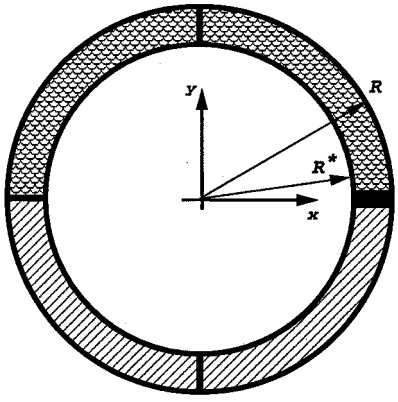

Figure 6. Finite element mesh used for the plane crack at a bi-material interface.

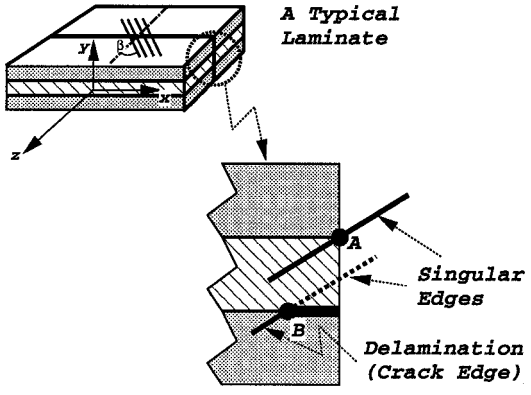

Figure 7. Cross-ply anisotropic laminate.

part and being denoted by $e_{\Re\alpha_{1,2}}$ and the other defining the relative error in the imaginary part $e_{\Im\alpha_{1,2}}$

$$e_{\Re\alpha_{1,2}}(\%) = 100\frac{\Re\alpha_1^{FE} - \Re\alpha_1}{\Re\alpha_1}, \quad e_{\Im\alpha_{1,2}}(\%) = 100\frac{\Im\alpha_1^{FE} - \Im\alpha_1}{\Im\alpha_1}. \tag{19}$$

We summarize the number of degrees of freedom, the CPU elapsed time[1] and the relative error (%) in the first 3 eigenvalues in Table 1. The results in Table 1 show that the method provides excellent results for complex eigen-pairs.

3.2. TWO CROSS-PLY ANISOTROPIC LAMINATE

We study edge singularities associated with a two cross-ply anisotropic laminate. Consider a composite laminate with ply properties typical of a high-modulus graphite-epoxy system, as shown in Figure 7. The orientation of fibers differs from layer to layer. Referring to the principle direction of the fibers, we define

$$E_L = 1.38 \times 10^5\,\text{MPa}(20 \times 10^6\,\text{psi}) \quad E_T = E_z = 1.45 \times 10^4\,\text{MPa}(2.1 \times 10^6\,\text{psi})$$

[1] Computations performed on a SGI Indigo^2 machine, with a R4400 200 Mhz processor, Specfp 92 = 131.

Table 1. Relative error (%) in the first 3 eigenvalues – Plane crack edge at a bi-material interface.

p-level	$p=1$	$p=2$	$p=3$	$p=4$	$p=5$	$p=6$	$p=7$	$p=8$
DOF	30	69	108	159	222	297	384	483
CPU (sec)	0.17	0.48	2.4	2.2	3.9	6.4	10.8	16.4
e-val #								
$e_{\Re\alpha_{1,2}}$	1.03	-0.196	-0.011	-0.00050	-0.000014	$5.2e-11$	-0.0000000028	-0.0000000025
$e_{\Im\alpha_{1,2}}$	-95	-15.5	-1.118	-0.0425	0.0010	-0.000017	0.000000013	0.000000079
e_{α_3}	2.59	0.0256	0.0001	0.00000028	-0.0000000015	0.0000000097	0.000000005	-0.000000035

$$G_{LT} = G_{Lz} = G_{Tz} = 0.586 \times 10^4\,\text{MPa}(0.85 \times 10^6\,\text{psi}) \quad \nu_{LT} = \nu_{Lz} = \nu_{Tz} = 0.21,$$

where the subscripts L, T, z refer to fiber, transverse and thickness directions of an individual ply, respectively. The material matrix $[E]$ for a ply with fibers orientation rotated by an angle β about the y-*axis* is given by

$$[E] = [T(\beta)]^T [E_0][T(\beta)],$$

where,

$$[T(\beta)] = \begin{pmatrix} s^2 & 0 & c^2 & 0 & 0 & c{\cdot}s \\ 0 & 1 & 0 & 0 & 0 & 0 \\ c^2 & 0 & s^2 & 0 & 0 & -c{\cdot}s \\ 0 & 0 & 0 & s & c & 0 \\ 0 & 0 & 0 & -c & s & 0 \\ -2c{\cdot}s & 0 & 2c{\cdot}s & 0 & 0 & s^2 - c^2 \end{pmatrix},$$

$$c \stackrel{\text{def}}{=} \cos(\beta), \qquad s \stackrel{\text{def}}{=} \sin(\beta),$$

$$[E_0] = V \begin{pmatrix} (1-\nu_{Tz}\nu_{zT})E_L & (\nu_{LT}+\nu_{Lz}\nu_{zT})E_T & (\nu_{zL}+\nu_{zT}\nu_{TL})E_L & 0 & 0 & 0 \\ & (1-\nu_{Lz}\nu_{zL})E_L & (\nu_{zT}+\nu_{LT}\nu_{zL})E_T & 0 & 0 & 0 \\ & & (1-\nu_{LT}\nu_{TL})E_z & 0 & 0 & 0 \\ & & & \frac{G_{Tz}}{V} & 0 & 0 \\ & & & & \frac{G_{Lz}}{V} & 0 \\ & & & & & \frac{G_{LT}}{V} \end{pmatrix}, \quad (20)$$

$$V \stackrel{\text{def}}{=} (1 - \nu_{LT}\nu_{TL} - \nu_{Tz}\nu_{zT} - \nu_{Lz}\nu_{zL} - 2\nu_{LT}\nu_{Tz}\nu_{zL})^{-1},$$

$$\nu_{TL} = \nu_{LT}\frac{E_T}{E_L}, \qquad \nu_{zT} = \nu_{Tz}\frac{E_z}{E_T}, \qquad \nu_{zL} = \nu_{Lz}\frac{E_z}{E_L}.$$

We first investigate the eigen-pairs associated with the singularities near the junction of the free edge and the interface, *edge* A in Figure 7, for a commonly used $[\pm\beta]$ angle-ply composite. Of course, the eigen-pairs depend on β and we chose $\beta = 45^\circ$ for which the first 12 exact non-integer eigen-pairs are reported in (Wang and Choi, 1981) with 8 decimal significant digits: $\alpha_1 = 0.974424342$, $\alpha_{2,3} = 1.88147184 \pm i0.23400497$, $\alpha_{4,5} = 2.5115263 \pm i0.79281732\ldots$

The two-element mesh shown in Figure 8 is used in our computation. We summarize the relative error (%) in the first 5 non-integer eigenvalues, the number of degrees of freedom before performing static condensation, and the CPU elapsed time required for the computation in Table 2. The rate of convergence of the eigen-values (reported in Table 2) is clearly visible when plotted on a log-log scale as shown in Figure 9. Again one obtains a rapid convergence rate. The three-dimensional eigen-function vector (displacement fields) associated with α_1 obtained at $p = 8$ is illustrated in Figure 10.

Table 2. Relative error (%) in the first 5 non-integer eigenvalues – Cross-ply anisotropic laminate.

p-level	$p=1$	$p=2$	$p=3$	$p=4$	$p=5$	$p=6$	$p=7$	$p=8$
DOF	18	39	60	87	120	159	204	255
CPU (sec)	0.12	0.23	0.48	0.92	1.54	2.41	4.19	6.08
e-val #								
e_{α_1}	−7.5	−0.44	−0.38	0.056	−0.018	−0.0067	−0.000825	−0.00006
$e_{\Re\alpha_{2,3}}$	−30.4	−15.21	−0.298	−0.228	−0.053	−0.0064	−0.0022	−0.00033
$e_{\Im\alpha_{2,3}}$	**	**	−15.71	−3.196	0.112	0.106	0.0077	−0.00004
$e_{\Re\alpha_{4,5}}$	−7.75	6.11	4.05	0.315	−0.187	−0.122	−0.013	−0.0034
$e_{\Im\alpha_{4,5}}$	**	**	−18.52	−11.43	−1.13	−0.041	0.073	0.0135

** - No imaginary part.

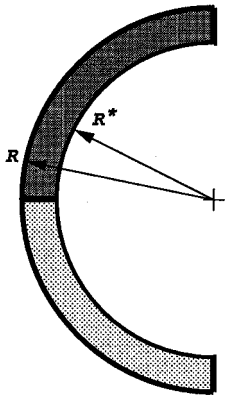

Figure 8. Finite element mesh used for the cross-ply anisotropic laminate.

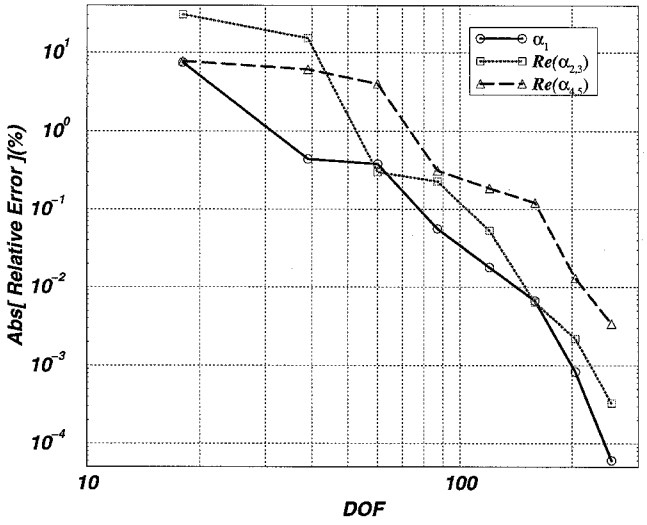

Figure 9. Convergence of approximated eigen-values for the cross-ply anisotropic laminate.

The variation of the eigen-values for different $[\pm\beta]$ cross-ply laminate is investigated in the following. We use the same mesh presented in Figure 8, with different material properties which reflect a laminate with fibers rotated at an angle $\pm\beta$ about the y-*axis*. The obtained eigen-values reported in Table 3 are accurate up to the 5 decimal digit shown. This accuracy is guaranteed because these digits have not been changed while increasing the polynomial level over the finite element mesh.

Table 3. Eigenvalues for different $[\pm\beta]$ fiber orientation cross-ply laminate.

$[\pm\beta]$	15°	30°	45°	60°	75°
α_1	0.99936	0.98834	0.97442	0.97665	0.99105

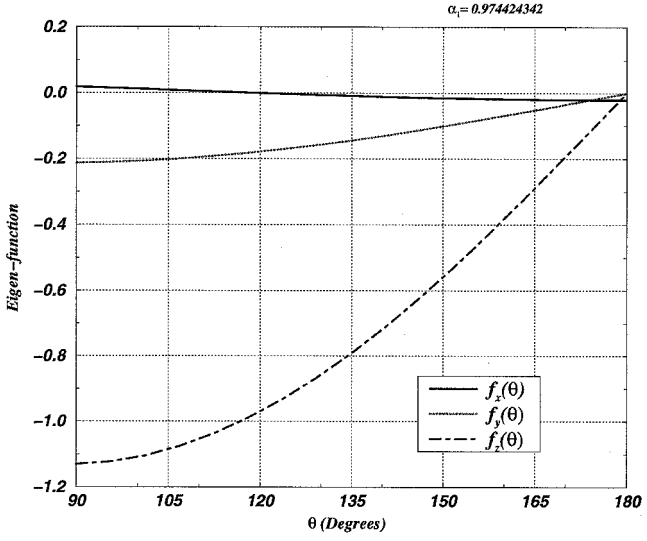

Figure 10. Eigen-functions associated with α_1 for the cross-ply anisotropic laminate.

Delamination: Once a crack starts propagating between two lamina, the behavior of the singular stress tensor changes dramatically, and the eigen-pairs are different. We consider a plane-crack with a tip at the edge denoted by *edge B* in Figure 7. Again we consider a $[\pm 45^\circ]$ cross-ply laminate, and use a four-element mesh (as the one in Figure 6) for the computations. The first three eigen-values and the number of DOFs at each p-level are summarized in Table 4. Observing the obtained results we may conclude with a high degree of confidence that $\alpha_{1,2} = 0.500000 \pm 0.0343$ and $\alpha_3 = 0.50000$.

3.3. Anisotropic multi-material internal interface

Figure 11 depicts a three material internal interface. Each of the three materials, denoted by I, II and III is the same fiber/resin composite. Composite's properties, when referring to the principle direction of the fibers, are

$$E_1 = E_3 = 0.105, E_2 = 1.0 \quad G_{12} = G_{13} = G_{23} = 0.0425,$$

$$\nu_{12} = 0.02205, \qquad \nu_{13} = 0.21, \qquad \nu_{23} = 0.21,$$

where the subscripts 1, 2, 3 refer to fiber, transverse and thickness directions of an individual composite, respectively. The material matrix $[E]$ for a ply with fibers orientation rotated by an angle θ_i about the x-*axis* is given by

$$[E] = [T(\theta_i)]^T [E_0][T(\theta_i)],$$

Table 4. First 3 eigen-values for a crack between two laminas in a cross-ply anisotropic laminate.

p-level	$p=1$	$p=2$	$p=3$	$p=4$	$p=5$	$p=6$	$p=7$	$p=8$
DOF	30	69	108	159	222	297	384	483
$\mathfrak{Re}\alpha_{1,2}^{FE}$	0.517095	0.498988	0.500189	0.4999305	0.499995	0.500005	0.500002	0.500000
$\mathfrak{Fe}\alpha_{1,2}^{FE} * 100$	3.472695	3.464185	3.518766	3.467100	3.444288	3.437041	3.435015	3.434454
α_3^{FE}	0.516157	0.510878	0.499144	0.499133	0.499847	0.500039	0.500020	0.500001

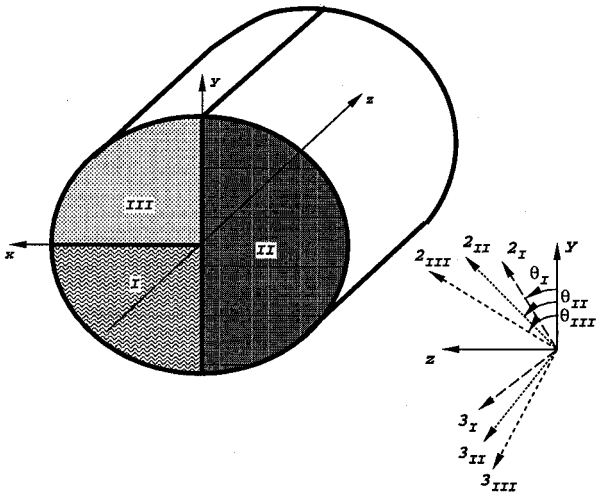

Figure 11. Anisotropic multi-material internal interface problem.

where in this case,

$$[T(\theta_i)] = \begin{pmatrix} 1 & 0 & 0 & 0 & 0 & 0 \\ 0 & c^2 & s^2 & 0 & c{\cdot}s & 0 \\ 0 & s^2 & c^2 & 0 & -c{\cdot}s & 0 \\ 0 & 0 & 0 & c & 0 & -s \\ 0 & -2c{\cdot}s & c{\cdot}s & 0 & c^2 - s^2 & 0 \\ 0 & 0 & 0 & s & 0 & c \end{pmatrix},$$

$$c \stackrel{\text{def}}{=} \cos(\theta_i), \qquad s \stackrel{\text{def}}{=} \sin(\theta_i)$$

and $[E_0]$ is given in (20). The fiber orientation of the three materials differ from each other, and are measured from the y-axis in the $y - z$ plane by the angles θ_{I}, θ_{II} and θ_{III} for the materials I, II and III, respectively.

This example problem is provided to show the ease with which the method can be used for complicated material arrangements, to demonstrate computation of eigen-pairs for an internal interface edge, and because numerical results are available in (Pageau and Biggers, 1996). For the case of $\theta_{\text{I}} = -\theta_{\text{III}} = -45°$, and $\theta_{\text{II}} = 0°$, we compute the first three eigen-pairs using the finite element mesh shown in Figure 12. Table 5 summarizes the first three eigen-values obtained while increasing the polynomial level over the elements from 2 to 8, and the relative error in percents between two consecutive eigen-values (computed at p and $p + 1$ polynomial levels). We may conclude with high confidence that the first three eigen-values, accurate within 6 significant figures are

$$\alpha_1 = 0.917456 \quad \alpha_2 = 0.981241 \quad \alpha_3 = 1.000000.$$

These values correspond well with the values $\alpha_1 = 0.915760$ and $\alpha_2 = 0.980782$ reported in (Pageau and Biggers, 1996) which are quoted to be accurate to within 0.5%. The three-dimensional eigen-function vector (displacement fields) associated with $\alpha_1 = 0.917456$

Table 5. First 3 eigen-values for an anisotropic multi-material internal interface, $\theta_{\rm I} = -\theta_{\rm II} = -45^\circ, \theta_{\rm II} = 0^\circ$.

p-level	$p=2$	$p=3$	$p=4$	$p=5$	$p=6$	$p=7$	$p=8$
$\alpha_1^{(p)}$	0.9053821	0.9158236	0.9172656	0.91746110	0.9174595	0.9174562	0.9174567
$\frac{\alpha_1^{(p)}-\alpha_1^{(p-1)}}{\alpha_1^{(p)}}(\%)$	5.6%	1.14%	0.16%	2.13 E-2%	−1.78 E-4%	−3.51 E-4%	4.89 E-5%
$\alpha_2^{(p)}$	0.9757487	0.9804715	0.9811786	0.9812417	0.9812423	0.9812410	0.9812412
$\frac{\alpha_2^{(p)}-\alpha_2^{(p-1)}}{\alpha_2^{(p)}}(\%)$	5.7%	0.48%	7.21 E-2%	6.43 E-3%	5.78 E-5%	−1.30 E-4%	2.00 E-5%
$\alpha_3^{(p)}$	1.0004755	1.0000212	0.9999787	0.9999999	0.9999999	0.9999999	1.0000000
$\frac{\alpha_3^{(p)}-\alpha_3^{(p-1)}}{\alpha_3^{(p)}}(\%)$	−0.87%	−4.54 E-2%	−4.24 E-3%	2.12 E-3%	7.97 E-6%	2.03 E-7%	1.39 E-9%

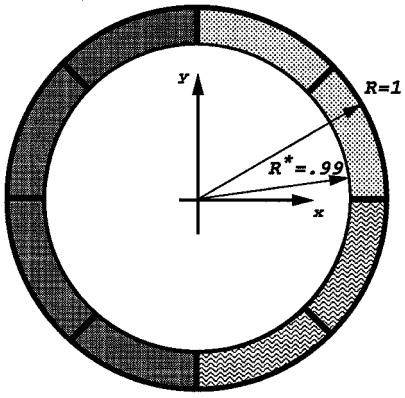

Figure 12. Finite element mesh used for the anisotropic multi-material internal interface.

obtained at $p = 8$ is illustrated in Figure 13. The eigen-function vector reported in Figure 14 in (Pageau and Biggers, 1996) is expressed in a polar co-ordinate system, and after transformation to the Cartezian co-ordinate system is very similar to the one presented in Figure 13. Since the exact eigen-functions are not available, one may question on the correctness of the reported eigen-function vector. To address this question an adaptive process has been adopted, and the residual has been computed. Namely, the eigen-stress tensor computed from the eigen-pairs has been substituted in the three first-order partial differential equations of equilibrium. Were the eigen-stress tensor exact, its substitution in the equilibrium equations would have satisfied the equations identically. However, because of the numerical errors, a residual is obtained, which converges to zero as the p-level is increased (a manuscript with detailed discussion and examples on *a-posteriori* error estimates for eigen-pairs computed numerically will be published in the future). At $p = 8$ the residual obtained for the first eigen-pair is less than 10^{-5} for all three equilibrium equations, for any angle, and at most angles is 10^{-8}. This *a-posteriori* estimation increases the confidence in the results.

We investigate the first three eigen-values when keeping $\theta_{\mathrm{I}} = -\theta_{\mathrm{III}} = -45^{\circ}$, and changing θ_{II} from 0 to 90 degrees. The third eigen-value (α_3) is 1.0 for all θ_{II}, so we summarize in Table 6 the first two eigen-values as θ_{II} changes. The behavior of the first two eigen-values, as a function of the angle θ_{II} is best illustrated in the graph presented in Figure 14. This demonstrates that when $\theta_{\mathrm{I}} = -\theta_{\mathrm{III}} = -45^{\circ}$, and $\theta_{\mathrm{II}} \approx 45^{\circ}$, complex eigen-pairs are obtained, and the stress-tensor has 'oscillatory singularity'. However, the strongest singularity is obtained at $\theta_{\mathrm{II}} = 0$.

3.4. Composite patch attached to a metallic structure

In recent years laminated composite patches have been used for the repair of aging aircraft with fatigue cracks. These patches are usually bonded to metallic structures and typically terminate at an angle γ as illustrated in Figure 15. We assume that the adhesive layer between the composite patch and the metallic structure has zero thickness, so that the composite is in full contact with the metal. Herein we investigate the edge singularities along the composite patch edge at the intersection of face A and B. The composite is taken to be the graphite-epoxy lamina with material properties as given in subsection 3.2, with fibers orientation rotated by an angle β about the y-axis. The metallic structure is AL7075-T6 with Young modulus

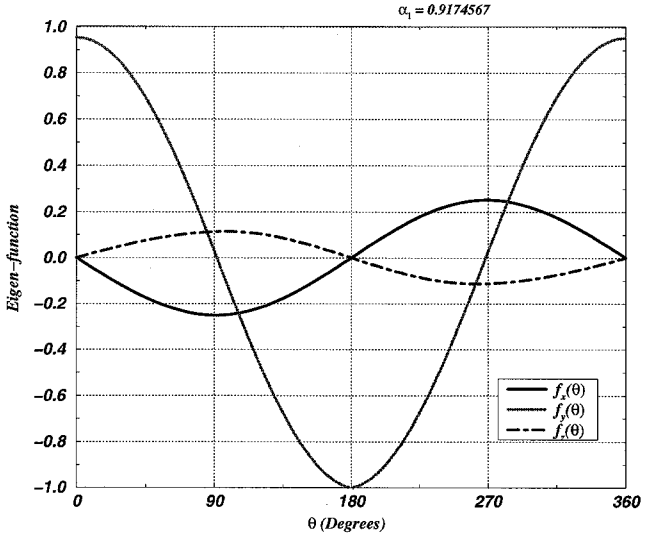

Figure 13. Eigen-function vector associated with α_1 for the anisotropic multi-material internal interface.

Table 6. First two eigen-values for an anisotropic multi-material internal interface, $\theta_{\rm I} = -\theta_{\rm III} = -45^\circ$, while $\theta_{\rm II} = 0^\circ$ to 90°.

$\theta_{\rm II}$	α_1	α_2
0°	0.91745669	0.98124118
10°	0.92115292	0.97998158
20°	0.93066075	0.97609411
30°	0.94231127	0.96948293
40°	0.95296001	0.96041106
41.5°	0.95471248	0.95856376
43°	$0.95655454 \pm i0.00173538$	
45°	$0.95639415 \pm i0.00268324$	
47°	$0.95618821 \pm i0.00260695$	
48.5°	$0.95601132 \pm i0.00202495$	
50°	0.95545474	0.95618789
60°	0.94876581	0.96048084
70°	0.95000906	0.95885802
80°	0.95337122	0.95759159
90°	0.94909612	0.96356568

$E = 7.17 \times 10^4$ MPa$(10.5 \times 10^6$ psi), and $\nu = 0.3$. The finite element mesh contains six elements, with two elements representing the composite and four elements representing the metal.

We first investigate the eigen-pairs obtained with fiber orientation $\beta = 45^\circ$ while changing the terminating angle γ from 20° to 90°. The first two eigen-values are summarized in Table 7, with α_3 being 1.0. It is interesting to remark that if the patch would have been made of AL7075-

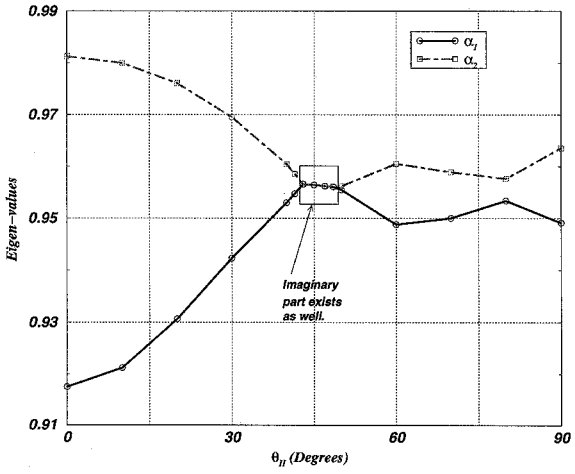

Figure 14. Variation of eigen-values as θ_{II} changes for an anisotropic multi-material internal interface, $\theta_{\mathrm{I}} = -\theta_{\mathrm{III}} = -45^{\circ}$.

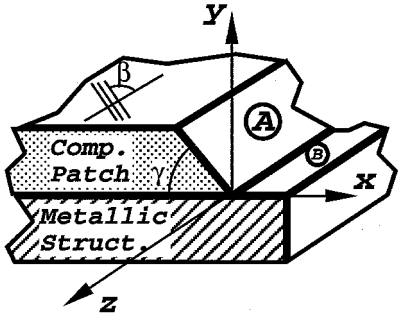

Figure 15. Composite patch attached to a metallic structure.

T6, and $\gamma = 90^{\circ}$, the first three eigen-values would be $\alpha_1 = 0.54448373, \alpha_2 = 0.66666667$ and $\alpha_3 = 0.90852919$, which give rise to a 'stronger' edge singularity.

We next investigate the influence of the fiber orientation, the angle β, on the eigen-values, while keeping $\gamma = 90^{\circ}$, and summarize in Table 8 the first three eigen-values. To visualize the influence of both the fiber orientation angle β, and the termination angle (γ) on the eigen-values, we present in Figure 16 two 3-D plots. These plots enable the visualization of the optimal combination of angles β and γ to produce the highest first two eigen-values. Equivalently, given the fiber orientation angle β, one may determine the terminating angle γ so as to obtain the maximum first eigen-value. For this example problem these angles may be easily realized intuitively without such 3-D plots, however, for complicated material combinations and geometries the intuitive answers may not be trivial. It is also interesting to remark that the third eigen-value is 1.0 for most angles $20^{\circ} \leqslant \gamma < 90^{\circ}$, except at $\gamma \approx 90^{\circ}$ (as seen in Table 8).

Table 7. First two eigen-values for the composite patch, $\beta = 45^\circ$, attached to a metallic structure, while $\gamma = 20^\circ$ to 90°.

γ	α_1	α_2
20°	0.82836708	0.96616009
30°	0.78665173	0.94669953
40°	0.75869470	0.92347722
50°	0.73757931	0.89475984
60°	0.71958205	0.85975886
70°	0.70233672	0.82065223
80°	0.68411600	0.78274434
90°	0.66418434	0.75085365

Table 8. First three eigen-values for the composite patch, $\gamma = 90^\circ$, attached to a metallic structure, while $\beta = 0^\circ$ to 90°.

β	α_1	α_2	α_3
0°	0.63637988	0.80945736	0.95767412
10°	0.63766263	0.80302942	0.96071226
20°	0.64161807	0.78792249	0.96721225
30°	0.64846848	0.77096564	0.97363849
40°	0.65829079	0.75641055	0.97871748
45°	0.66418434	0.75085365	0.98071187
50°	0.67048739	0.74692325	0.98236759
60°	0.68248688	0.74642680	0.98475523
70°	0.68962767	0.76087624	0.98607408
80°	0.69167996	0.78946576	0.98656827
90°	0.69201351	0.80945736	0.98661486

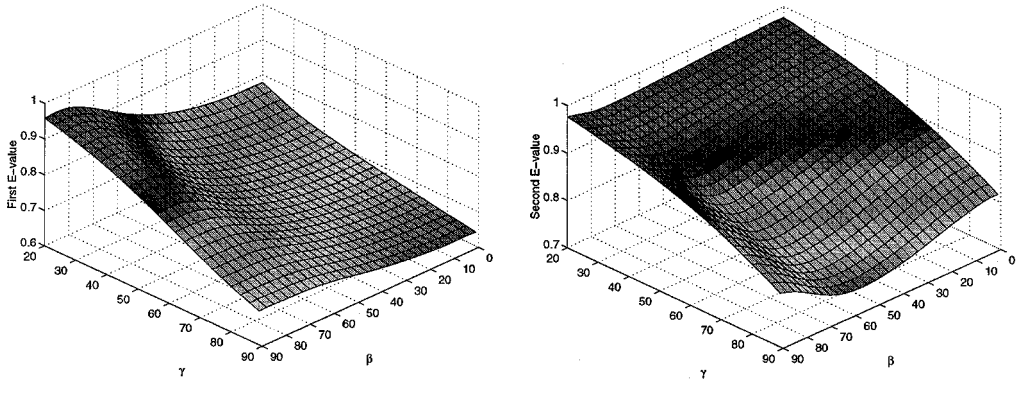

Figure 16. First two eigen-values as a function of the fiber orientation angle (β), and terminating angle γ for the composite patch attached to a metallic structure.

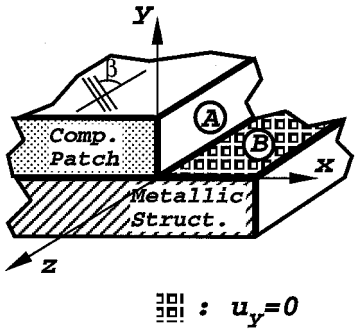

Figure 17. Composite patch attached to a metallic structure, constrained against vertical movement.

3.5. COMPOSITE PATCH ATTACHED TO A METALLIC STRUCTURE CONSTRAINED AGAINST MOVEMENT

We consider herein a similar composite patch attached to a metallic structure, only that the metallic structure is constrained against movement in the vertical direction immediately where the patch ends. Referring to Figure 17, we assume that face A of the patch is traction free, while face B (which belongs to the metallic structure) is constrained: $u_y = 0$, but $T_x = 0$ and $T_z = 0$. This situation is a typical representation of a patched aluminum plate in the vicinity of a titanium beam (as the wing skin in an aircraft between two main beams). A five element-mesh is used, having two elements representing the composite patch and three elements representing the AL7075-T6 metallic structure. The p-level over the elements is increased from 1 to 8, observing an excellent convergence of the eigen-values. The first three eigen-values at p-level $= 8$, for fiber orientation angles β from 0° to 90° are plotted in Figure 18. It is interesting to observe that the first eigen-value is almost independent of β, and is smaller than 0.5 (first eigen-value corresponding to a crack tip); thus, the singularity of this configuration is more severe than a crack tip. Also, were the patch made of the same material as the metallic structure (AL7075-T6), the first eigen-value would have been $\frac{1}{3}$, giving rise to a more severe singularity.

4. Conclusions

A numerical method for reliable computation of three-dimensional edge eigen-pairs in anisotropic domains, based on the modified Steklov formulation and the p-version of the FEM, has been described. The method is very general in that it is applicable to many kinds of edge singularities, and it has been demonstrated on several problems including reentrant-corners, abrupt changes in material properties or boundary conditions, and internal material interfaces. Although some of the example problems have been treated in the past (and have been used for comparison purposes), many new results are presented as well. The numerical experiments indicate that the computed values converge strongly, are accurate and inexpensive from the points of view of human time needed for input data preparation, and required CPU time.

Power-logarithmic stress singularities could be detected by monitoring the two computed distinct but adjacent eigenvalues and their corresponding eigen-functions. When these collapse into one as the number of degrees of freedom is increased, this indicates the presence of these kind of singularities. This has been demonstrated in a 2-D setting in (Yosibash, 1997a).

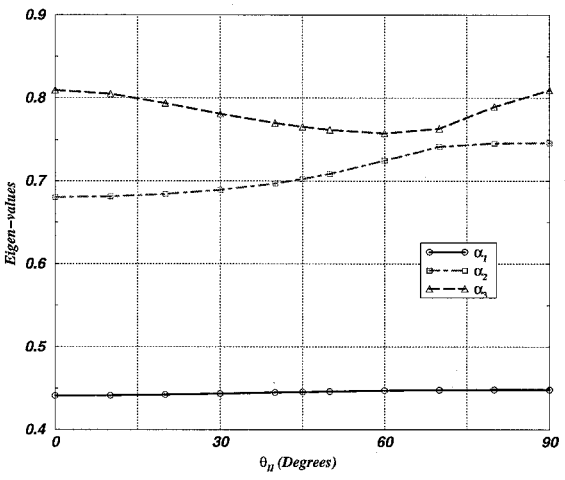

Figure 18. First three eigen-values as a function of the fiber orientation angle (β), for the constrained metallic structure.

Investigation of edge singularities is important because it provides a rigorous quantitative basis for investigating failure events, such as delamination of composite materials, and failure in electronic devices. The edge eigen-pairs are the first step in a general method which is intended to provide also the series coefficients, namely the edge stress intensity functions (ESIFs). The obtained eigen-pairs are used for extracting the ESIFs by methods as the complementary energy method (described in (Szabó and Yosibash, 1996) in a 2-D setting), and this will be reported in a following paper.

Acknowledgement

The author thanks an anonymous referee for his valuable comments and for pointing out a mistake in one of the subsections in an earlier stage of the manuscript. The reported work has been partially supported by the AFOSR under STTR/TS project No. F-49620-97-C-0045.

References

Anderson, E., Bai, Z., Bischof, C., Demmel, J., Dongarra, J., Du Croz, J., Greenbaum, A., Hammarling, S., McKenney, A., Ostrouchov, S. and Sorensen, D. (1994). *LAPACK Users' Guide - Release 2.0.* SIAM.

Andersson, B., Falk, U., Babuška, I. and Von-Petersdorff, T. (1995). Reliable stress and fracture mechanics analysis of complex components using a h-p version of FEM. *International Journal for Numerical Methods in Engineering* **38**, 2135–2163.

Babuška, I. and Aziz, A.K. (1972). Survey lectures on the mathematical foundations of the finite element method. *The Mathematical Foundations of the Finite Element Method with Applications to Partial Differential Equations* (Edited by A.K. Aziz), Academic Press, New York, NY, USA, 3–343.

Barsoum, R. (1988). Theoretical basis of the finite element iterative method for the eigenvalue problem in stationary cracks. *International Journal for Numerical Methods in Engineering* **26**, 531–539.

Bogy, D.B. and Wang, K.C. (1971). Stress singularities at interface corners in bonded dissimilar isotropic elastic materials. *International Journal of Solids and Structures* **7**, 993–1005.

Costabel, M. and Dauge, M. (1995). Computation of corner singularities in linear elasticity. *Boundary Value Problems and Integral Equations in Nonsmooth Domains* (Edited by M. Costabel, M. Dauge and S. Nicaise), Marcel Dekker, New York, Basel, Hong-Kong, 59–68.

Dauge, M. (1988). *Elliptic Boundary Value Problems in Corner Domains – Smoothness and Asymptotics of Solutions*. Lecture notes in Mathematics 1341, Springer-Verlag, Heidelberg.

Dempsey, J.P. and Sinclair, G.B. (1979). On the stress singularities in the plane elasticity of the composite edge. *Journal of Elasticity* **9**(4), 373–391.

Dempsey, J.P. and Sinclair, G.B. (1981). On the singular behavior at the vertex of a bi-material wedge. *Journal of Elasticity* **11**, 317–327.

Grisvard, P. (1992). *Singularities in Boundary Value Problems*, Masson, France.

Gu, L. and Belytschko, T. (1994). A numerical study of stress singularities in a two-material wedge. *International Journal of Solids and Structures* **31**(6), 865–889.

Hein, V.L. and Erdogan, F. (1971). Stress singularities in a two-material wedge. *International Journal of Fracture* **7**(3), 317–330.

Leguillon, D. and Sanchez-Palencia, E. (1987). *Computation of Singular Solutions in Elliptic Problems and Elasticity*, John Wiley & Sons, New York, NY.

Pageau, S.S. and Jr. Biggers, S.B. (1996). A finite element approach to three dimensional singular stress states in anisotropic multi-material wedges and junctions. *International Journal of Solids and Structures* **33**, 33–47.

Pageau, S.S., Joseph, P.F. and Jr. Biggers, S.B. (1995). Finite element analysis of anisotropic materials with singular inplane stress fields. *International Journal of Solids and Structures* **32**(5), 571–591.

Papadakis, P. and Babuška, I. (1995). A numerical procedure for the determination of certain quantities related to stress intensity factors in two-dimensional elasticity. *Computer Methods in Applied Mechanics and Engineering* **122**, 69–92.

Szabó, B.A. and Babuška, I. (1991). *Finite Element Analysis*, John Wiley & Sons, New York.

Szabó, B.A. and Yosibash, Z. (1996). Numerical analysis of singularities in two-dimensions. Part 2: Computation of the generalized flux/stress intensity factors. *International Journal for Numerical Methods in Engineering* **39**(3), 409–434.

Ting, T.C.T. (1986). Explicit solution and invariance of the singularities at an interface crack in anisotropic composites. *International Journal of Solids and Structures* **22**(9), 965–983.

Ting, T.C.T. and Chou, S.C. (1981). Edge singularities in anisotropic composites. *International Journal of Solids and Structures* **17**(11), 1057–1068.

Wang, S.S. and Choi, I. (1982). Boundary layer effects in composite laminates: Part 1 – free edge stress singularities. *Transaction ASME, Journal of Applied Mechanics* **49**, 541–548.

Williams, M.L. (1952). Stress singularities resulting from various boundary conditions in angular corners of plates in extension. *Transaction ASME, Journal of Applied Mechanics* **19**, 526–528.

Ying, X. (1986). *A Reliable Root Solver for Automatic Computation with Application to Stress Analysis of a Composite Plane Wedge*, PhD thesis, Washington University, St. Louis, Missouri, USA.

Yosibash, Z. (1997a). On solutions of two-dimensional linear elastostatic and heat-transfer problems in the vicinity of singular points. *International Journal of Solids and Structures* **34**(2), 243–274.

Yosibash, Z. (1997b). Numerical analysis of edge singularities in three-dimensional elasticity. *International Journal for Numerical Methods in Engineering* (in press).

Yosibash, Z. and Szabó, B.A. (1995). Numerical analysis of singularities in two-dimensions. Part 1: Computation of eigen-pairs. *International Journal for Numerical Methods in Engineering* **38**(12), 2055-2082.